ACS Sustainable Chemistry & Engineering

pubs.acs.org/journal/ascecg

Research Article

Turning Recycled Cardboard Container-Derived Lignin-Containing Cellulose Nanofibrils into a Robust Gas Barrier UV-Shielding Film

Ikramul Hasan, Jinwu Wang, Douglas Bousfield, and Mehdi Tajvidi*

Cite This: *ACS Sustainable Chem. Eng.* 2023, 11, 3720−3731

Read Online

ACCESS | Metrics & More | Article Recommendations | Supporting Information

ABSTRACT: Self-standing cellulose nanofibril (CNF) films are regarded as one of the promising alternatives to current petroleum-based packaging materials mostly due to their ability to form dense self-assembled structures exhibiting high gas barrier properties. Nonetheless, one of the major obstacles to the commercialization of these materials in packaging applications is the high cost of raw materials and production energy. In this study, we created self-standing films of lignin-containing cellulose nanofibrils (LCNFs) derived from a recycled old corrugated cardboard (OCC) pulp that costs less than bleached softwood Kraft (BSK) pulp and requires half as much energy for refining to obtain the same quality of material. The low zeta potential (−3.83 mV) of OCC-derived LCNFs (OCC-LCNFs) resulted in aggregation of the fibrils in aqueous suspension, leading to considerable unpredictability in oxygen permeability (OP) values (coefficient of variation 36%). The addition of 3 wt % (based on the dry weight of LCNFs) carboxymethyl cellulose lowered the coefficient of variation to 16% with an average OP of 1478 (cc.μm/m^2.atm.day) at 80% relative humidity. Because the OP was higher than that of the CNF film made from BSK-derived CNF (BSK-CNFs), we demonstrated that ionic crosslinking with trivalent aluminum ion or covalent crosslinking with polyamide epichlorohydrin decreased the OP by 30% at 23 °C and 80% relative humidity while also significantly enhancing the tensile strength and modulus. In addition, the presence of lignin in OCC resulted in a relatively lower water vapor permeability value in OCC-LCNF films compared to BSK-CNF films. Moreover, OCC-LCNF films showed complete UV-shielding (200−400 nm) property. Overall, this work provides a new opportunity to exploit a recycled and inexpensive source of CNFs to produce robust gas barrier materials for packaging applications.

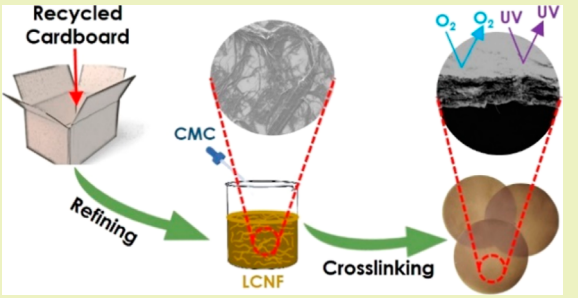

KEYWORDS: *cellulose nanofibrils, crosslinking, packaging, gas barrier, UV-blocking*

INTRODUCTION

High gas barrier property is desired for polymeric materials in the domain of flexible electronics and food packaging.[1−3] Traditionally, a thin layer of the metal coating (usually aluminum) on the polymer film is commercially used to impart high gas barrier properties.[4] This approach not only leaves a high carbon footprint but also makes the recycling of plastic materials difficult if not impossible. Petroleum-sourced polymers blended with different inorganic nanoclays[5] or 2D nanosheets[6] to make nanocomposites either in a single layer[7] or in a multilayer[8] are currently researched to attain high gas barrier properties. However, multilayer films have a serious issue with end-of-life disposal and recycling as commonly used mechanical recycling is not compatible with them, and it requires complex solvent-targeted recovery, followed by precipitation.[9] On the other hand, research on single-layered composites still has compatibility issues between the matrix (polymers) and filler (usually inorganic materials including clay), and most of the fillers are not commercially viable.[10,11] Above all, most polymers are manufactured from non-renewable sources and have serious environmental impact if littered.

Cellulose nanofibrils (CNFs), a form of cellulose nanomaterials (CNMs) with a high aspect ratio (usually >100), have gained a considerable amount of attention in the research community as they can form dense self-assembled structures from their suspension attributed to strong capillary forces, hydrogen bonding, and London dispersion forces, resulting in high gas barrier properties as well as mechanical strength.[12] The traditional CNF production process involves the chemical pulping of softwood chips followed by a bleaching process to obtain the so-called bleached softwood Kraft (BSK) pulp and subsequent size reduction by mechanical disintegration through high shear forces.[13] BSK-derived CNFs (BSK-CNFs) are mostly pure cellulose as nearly all lignin and hemicellulose are removed during the chemical pulping process. There are many research articles already available on

Received: November 7, 2022
Revised: February 10, 2023
Published: February 22, 2023

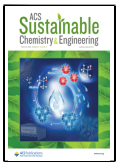

the high gas barrier application of neat self-standing CNF films[14] as well as blended[15,16] or layered[17,18] nanocomposites with other biobased polymers and clay materials. Whatever the case, the commercialization of CNF-based materials is still a big challenge due to the high cost of raw materials (e.g., BSK) and energy-intensive production processes (e.g., homogenization, refining, and grinding). Alternative non-woody sources like bast fibers,[19] fruit stalks,[20] and agricultural residues of different crops[21,22] are also studied as inexpensive sources. However, all those sources are not still commercially available on a large scale and require chemical and mechanical pretreatment even before nanofibrillation, thereby increasing the ultimate cost of CNF production.

Paper-based packaging materials like old corrugated containers (OCCs) have been recycled for a long time to minimize waste generation as well as the production cost of packaging materials. Although the consumption of OCCs in the United States consistently increased from 2013 with a recent demand hike due to the pandemic, the OCC waste export is significantly decreased due to recent market development and complete Chinese prohibition on solid waste import.[23] As a result, OCC waste recycling and upcycling have become a crying need for the US economy and environment and can be an excellent source of CNF production. A recycled OCC is almost 10 times lower in cost than the BSK pulp, can be easily repulped, and consumes nearly half of the energy for refining compared to BSK pulp.[24] On the other hand, an OCC is generally produced from recycled fibers that are not usually bleached and goes through the recycling process multiple times, making the OCC-derived lignocellulosic nanofibrils (LCNFs) a more sustainable option.[25] Very recently, some research groups extracted LCNFs from OCCs through mechanical defibrillation and used in paper, paperboard, and film making applications.[26−28] All those works are based on lab-based small-scale fibrillation processes. Copenhaver et al. first produced LCNFs from recycled OCCs through the pilot-scale refiner at the University of Maine and reported the energy demand for a different fines content of LCNF.[24] They also showed the reinforcement property of OCC-LCNFs in the polymeric matrix. While composite and paperboard applications of OCC-LCNFs have been explored, the gas barrier performance of such materials is yet to be understood, which is critically important for the commercialization of these nanofibrils. Moreover, due to the presence of different additives, the interfibrillar attraction of fibrils present in OCC-LCNFs is expected to be interrupted, and thus, the gas barrier performance can be lost. As a result, we envisioned that a crosslinking strategy of the fibrils would improve the gas barrier performance of the OCC-LCNF films to the level of the gas barrier performance of films made from BSK-CNFs.

In this study, we report the gas barrier and mechanical properties of neat self-standing films made from OCC-derived LCNFs for the first time. In the beginning, we stabilized the colloidally unstable OCC-LCNF suspension through the addition of carboxymethyl cellulose (CMC) to obtain consistent oxygen permeability (OP) values. Then, we utilized the chemistry of an ionic interaction by trivalent Al^{3+} ions and covalent bonding by polyamide epichlorohydrin (PAE) to enhance the fiber−fiber interaction to improve the water vapor and oxygen barrier properties at a high relative humidity (80%) and compared the changes in properties between the ionic interaction and covalent bonding. We revealed the chemical composition and morphological changes induced by the crosslinking and related them to the properties. The thermal stability of the produced films was also investigated through thermogravimetric analysis. Finally, the UV-shielding ability and visible light transmittance of the films were analyzed and reported.

MATERIALS AND METHODS

Materials. Lignin-containing cellulose nanofibrils (LCNFs) were produced from the recycled pulp sourced from an old corrugated cardboard at the Process Development Center (PDC), University of Maine, following their patented process for CNF production.[29] The OCC fibers are sent through a refiner with specialized plates to highly fibrillate the fibers. They supplied the LCNFs as 3 wt % solid suspensions with a fines content of 70%. The fines content is defined as the percentage of particles with a length less than 200 μm as measured by a Morfi Analyzer (Techpap, France). The LCNFs were further ground to 90% fines content using a fine friction grinder (Super Masscolloider, Model: MKCA6-2, Masuko Sangyo, Kawaguchi, Japan) at 2200 rpm, and the final concentration was 2 wt %. The clearance between the stationary and rotary grinding discs was set to −20 μm after determining the zero gap. The 70% LCNF slurry was recirculated through the system, allowing multiple grinding passes until a fines content of 90% was achieved. The produced LCNFs contained 16.7% residual lignin and 18.1% hemicellulose along with 61.9% cellulose.[30] A detailed morphological analysis of OCC-LCNFs from scanning electron microscopic images is provided in the Supporting Information (Figure S1). The width of the fibrils was measured using an image analysis technique by ImageJ (NIH, USA) software. The width of at least 50 fibrils was measured to obtain the average width of the fibrils from each of the image. BSK-CNFs were also provided from the PDC in a standard 3 wt % solid content and 90% fines content form, and the details about the morphology of these fibrils can be found in our previous work.[31] CMC sodium salt (repeat unit, n = 500; sodium content = 7.2%; and etherification value = 0.7) was purchased from Tokyo Chemical Industry Co. Ltd. (Tokyo, Japan) in a powder form. PAE (Polycup 9250, solid content = 20%) was kindly donated by Solenis LLC (Wilmington, DE). Liquid aluminum sulfate ($Al_2(SO_4)_3$), also known as alum in the paper industry, was supplied as an aqueous solution containing 48.5% $Al_2(SO_4)_3.14H_2O$ by Chemtrade Logistics Inc. (Ontario, Canada).

ζ Potential and Shear Flow Measurement. The ζ potential of all the suspensions was measured by a Malvern Zetasizer (Malvern Panalytical, UK). The solid content of each suspension was very low (~0.01%). The CNF suspension was diluted to 0.01 wt % from its original 3 wt % solid using deionized water. From each sample, at least three measurements were taken to get an average ζ potential of the overall suspension. The rheological properties of all suspensions with 0.5 wt % solid content were measured using an oscillating Discovery HR-2 hybrid rheometer (TA Instruments, DE, USA) with a cone plate geometry (angle: 2° 0′ 29″, diameter: 40 mm) at 23 °C. Frequency sweep data at 1% strain was recorded by taking 600 μL of suspension for each measurement and maintaining a geometry gap of 60 μm. Finally, complex viscosity was calculated using the instrument software.

Film Preparation. The films were prepared by the vacuum filtration method. First, the OCC-LCNF suspension was diluted to a 0.5 wt % solid containing suspension. Then, 3 wt % CMC (based on the dry mass of OCC-LCNFs) was added to the suspension and sonicated for 2 min with 20% output power by a Branson 450 Sonifier (Ultrasonics Corporation, Danbury, CN, USA). The CMC was expected to assist dispersing to OCC-LCNFs in the suspension and helped form a uniform film, which will be explained in the Results and Discussion section. The suspension was then vacuum-filtered at a suction pressure of 254 mm (Hg) on a polyester filter with an average pore size of 41 μm and a diameter of 11 cm until the time gap between two consecutive drops from the funnel was at least 20 s. The filtration time for 3 wt % CMC-added suspension was 15 ± 1 min. The wet film was then placed between two blotting paper and cold-pressed for 10 min to reduce the water content to ~50%, impregnated

https://doi.org/10.1021/acssuschemeng.2c06683
ACS Sustainable Chem. Eng. 2023, 11, 3720−3731

Scheme 1. Schematic Diagram of the OCC-Derived LCNF Films through Crosslinking with PAE or Al^{3+}

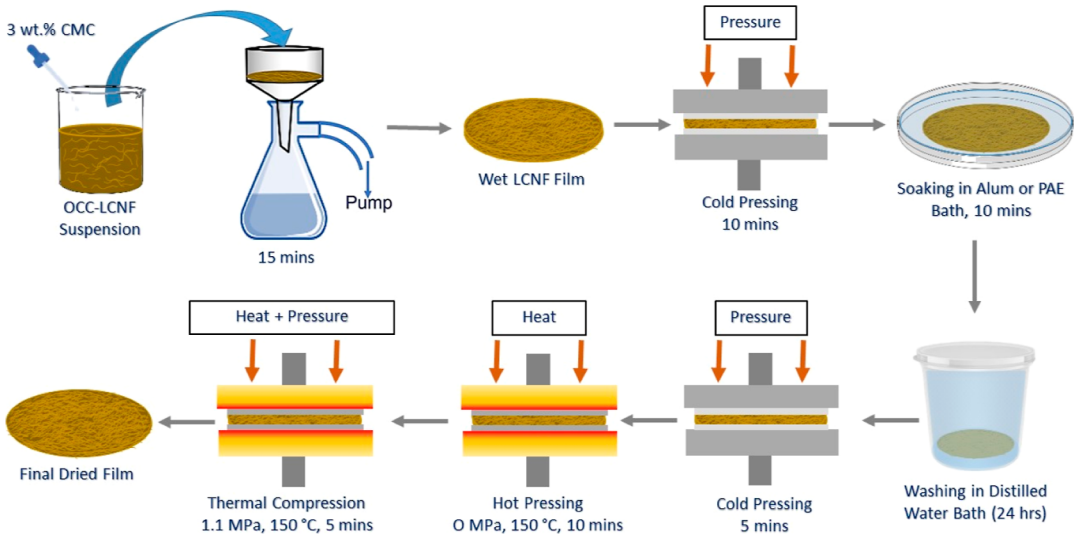

for 10 min in either 50 g of alum or PAE baths containing 0.1, 0.3, or 0.5 wt % for crosslinking, rinsed, and left in a distilled water bath for 24 h so that the unadsorbed Al^{3+} or PAE could leach out. After washing, the wet film was again cold-pressed for 5 min to reduce the water content again so that hot-press drying can be performed without the need of any water-absorbing substrate like paper. For the hot-press drying, the wet film was placed between two stainless steel plates and dried for 10 min at 150 °C without imparting any measurable pressure; that is, the platens were just in contact reading zero pressure. After hot-press drying, the films were further hot-pressed at high pressure (1.1 MPa) and 150° for 5 min. The reason for this second hot-pressing was to minimize the interlamellar gap in films, which was explained in detail in our previous work.[31] A schematic diagram of the film preparation process is shown in Scheme 1. All films were conditioned for at least 24 h at 23 °C and 50% relative humidity before any measurements.

Physical and Surface Properties. *Density.* For density measurement, all conditioned films were cut into specific diameter circles (9 cm) with a circle cutter, and the thickness of each film was measured with a micrometer (accuracy level = 0.001 mm). At least 10 measurements were taken to obtain the average thickness value. From the thickness and diameter of each film, the volume was calculated, and then the weight of each film was divided by the corresponding volume to calculate the final density of each film. At least, three density data were recorded for each sample.

Equilibrium Moisture Content. The equilibrium moisture content (EMC) at 50% relative humidity and 23 °C was measured by using a simple gravimetric technique to have a relative idea on the moisture content in alum and PAE crosslinked films. First, the films were dried in an oven at 120 °C for 1 h, and the dry weights (W_{dry}) were recorded. Then, the dry films were conditioned at 23 °C and 50% relative humidity for 48 h, and the weights (W_{moist}) of moisture-absorbed films were recorded. The EMC was calculated from eq 1

$$\mathrm{EMC}(\%) = \frac{W_{moist} - W_{dry}}{W_{dry}} \times 100\% \quad (1)$$

Surface Free Energy. A Kruss mobile surface analyzer (Hamburg, Germany) was used to measure the surface free energy (SFE) of each sample using the double-sessile drop technique. In this technique, 1 μL of liquid water (as a polar probe) or diiodomethane (as a non-polar probe) was dropped onto the surface of the films, and contact angles were measured after 2 s. From these two contact angles, surface free energies were calculated using the Owens, Wendt, Rabel, Kaelble (OWRK) method.[31] At least 10 measurements were taken from each sample to calculate an average value of water contact angle (WCA) and SFE.

Mechanical Testing. Tensile testing was performed for all the prepared samples. Each sample was cut into 5 cm × 1 cm strips before testing. An Instron 5942 Universal Mechanical Testing Machine (Instron, MA, USA) was used for tensile testing with a 500 N load cell. The test was performed at a gauge length of 2 cm and a displacement rate of 2 mm/min. Currently, there are no standard test methods for mechanical characterization of CNF and LCNF films, but our testing protocols are consistent with our previous work and other published data. The tensile strength, tensile strain at break, and tensile modulus were calculated from the recorded force−displacement curves. For the wet strength measurement of films, similar parameters and strip size were used. The strips were soaked in water for 1 h, and then excess water was removed with blotting paper and then tested immediately in Instron.

Water Vapor Permeability. The water vapor transmission rate (WVTR) was measured with a simple gravimetric technique following a modified ASTM E96/E96M-16 procedure. The process involved measuring the weight loss of a mason jar within a 24 h time difference that indicated the moisture loss through the film (Δ_{mass}). Initially, 60 g of water was added to the jar, and the top of the jar was covered with circular films with a diameter of 65 mm (radius, r = 32.5 mm). A metal cap and a silicone rubber gasket were used to lock and seal the film firmly. Then, the jar was kept in a conditioning chamber with 50% relative humidity at 23 °C. The initial weight of the jar was taken after 48 h so that the films had enough time to reach the steady state, and the second weight was taken after 1 day from the initial weighing. The WVTR can be calculated using eq 2

$$\mathrm{WVTR} = \frac{\Delta_{mass}}{\Pi r^2 .\ \mathrm{day}}\left(\frac{g}{\mathrm{m}^2\cdot\mathrm{day}}\right) \quad (2)$$

The WVTR water vapor permeability (WVP) was calculated from WVTR through eq 3 using the thickness of the film and the partial pressure difference of water vapor across the film.

$$\mathrm{WVP} = \mathrm{WVTR} \times \frac{\mathrm{thickness} \times 100}{P_{saturated} \times \Delta_{RH\%}}\left(\frac{\mathrm{g.\ mm}}{\mathrm{m}^2\cdot\mathrm{day}\cdot\mathrm{kPa}}\right) \quad (3)$$

where $P_{saturated}$ indicates the saturated vapor pressure (2.81 kPa) of water at 23 °C and $\Delta_{RH\%}$ indicates the difference in relative humidity inside (100%) and outside (50%) of the jar. The test for each sample was replicated with two different specimens to get the average WVP values.

Oxygen Permeability. The oxygen transmission rate (OTR) of the films was measured according to the ASTM D3985-17 method with a Mocon Ox-Tran 2/22 oxygen permeation analyzer at 23° and 80% relative humidity. All films were conditioned at 23 °C and 80%

https://doi.org/10.1021/acssuschemeng.2c06683
ACS Sustainable Chem. Eng. 2023, 11, 3720−3731

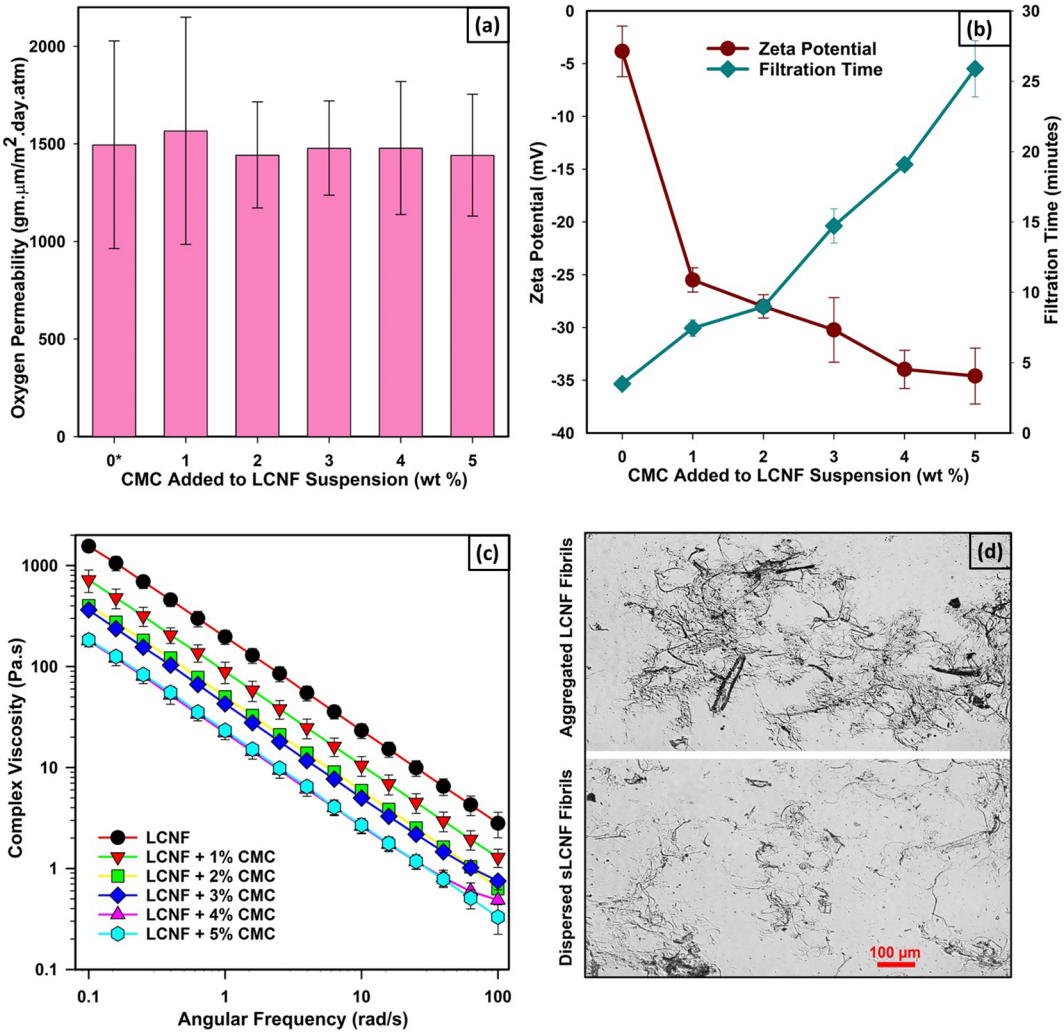

Figure 1. (a) OP values of the pure LCNF film (* indicates the values that were under the detection limit of the machine) and CMC-treated LCNF films at different concentrations; (b) with the addition of CMC zeta potential decreased and filtration time increased; (c) complex viscosity versus angular frequency graph showing shear thinning behavior of LCNF suspension with and without the addition of CMC; and (d) optical microscopic images of pure LCNFs and 3 wt % CMC-added LCNFs (sLCNF) dried from similar concentrations.

relative humidity for 24 h before testing. The testing process involved placing the circular films onto a cartridge with a testing area of 5.64 cm^2 and conditioning them again for 6 h inside the instrument at 80% relative humidity. The analyzer recorded the OTR values every 15 min and cleaned the sensor with a gas mixture of 98% N_2 and 2% H_2 for 15 min after two consecutive values and continued testing until the differences among the last five OTR values were less than 1% (convergence method). Then, the OTR values were thickness-normalized to obtain the OP values. Three specimens from each type of film were tested to obtain the average OP values with standard deviation.

Microscopic Analysis. A scanning electron microscope (SEM) (NVision 40, Zeiss, Germany) was utilized to observe the microscopic structure of the film surfaces and cross-sections. All specimens were sputter-coated with Au/Pd for 4 nm to avoid charge accumulation. For the cross-sections, the films were freeze-fractured with liquid nitrogen and then sputter-coated. The images were taken at various magnifications with a working distance ranging from 5 to 8 mm at 3 kV voltage.

Spectroscopic Analysis. *Fourier Transform Infrared.* Attenuated total reflection (ATR) infrared (IR) spectroscopy was performed on the films to characterize the functional groups present in the films and the possible changes in them after crosslinking. A PerkinElmer Spectrum Two Fourier transform infrared (FTIR) spectrophotometer was employed for the scanning range from 4000 to 450 cm^{-1} with a spectral resolution of 4 cm^{-1}. A total of 32 scans were performed on each specimen and combined in Spectrum 10 (PerkinElmer) software to obtain the average. All the obtained spectra were baseline-corrected and normalized against the intensity of the peak at 1024 cm^{-1} using the same software.

Ultraviolet/Visible. The films' transmittance in the visible region of the spectrum (400−800 nm), as well as the ultraviolet region (200−400 nm), was measured using a Lambda 365 + PerkinElmer double beam spectrophotometer. The machine had an internal setup to hold and measure the transparency of films and did not require a cuvette or a sample holder for measurement.

Statistical Analysis. Analysis of variance (ANOVA) was performed to analyze the effect of crosslinker type and the concentration of the crosslinker bath on the mechanical and barrier properties. All the analysis was performed by the IBM SPSS 28 (IBM Corporation, NY) with a level of significance of 0.05. Duncan's post hoc analysis was also run by the same software to classify the effects based on their group means.

RESULTS AND DISCUSSION

Addition of CMC to LCNF Suspension. Being a recycled material in nature, OCC-LCNFs contained a complex composition of organic and inorganic materials.[24] Although the LCNFs derived from wood pulp were reported to contain

https://doi.org/10.1021/acssuschemeng.2c06683
ACS Sustainable Chem. Eng. 2023, 11, 3720−3731

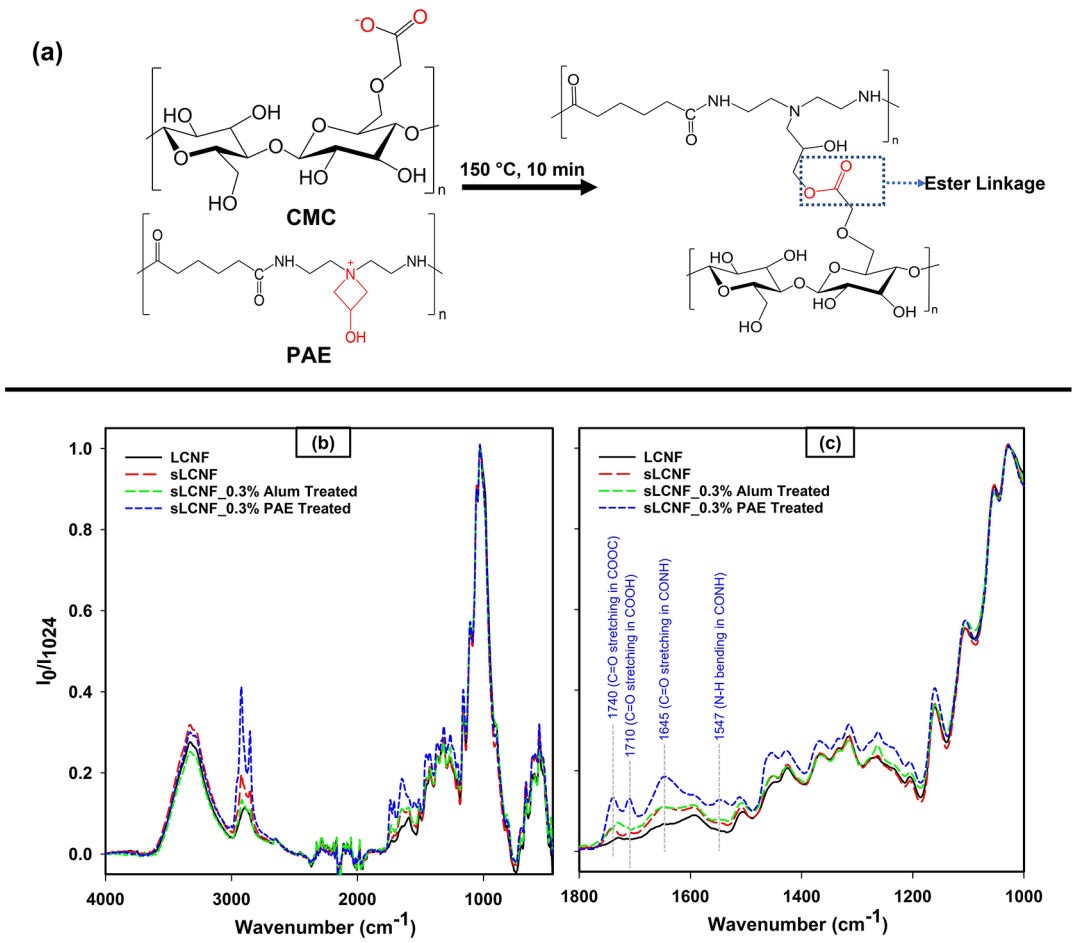

Figure 2. Schematic of one possible thermally induced crosslinking reaction between CMC and PAE (a) and the corresponding FTIR spectra at full scale (4000−450 cm^{-1}) (b) and the scale (c) of interest for crosslinking (1800−1000 cm^{-1}) for LCNF, 3 wt % CMC-stabilized LCNFs (sLCNFs), and sLCNFs treated in 0.3 wt % alum or 0.3 wt % PAE bath.

some surface charge,[32] OCC-LCNFs were found to have a small zeta potential of −3.83 mV in this study, indicating a low amount of surface charge. This low surface charge can be attributed to the incorporation of different additives and minerals during the OCC manufacturing process. Additionally, the pulp for LCNFs does not undergo a bleaching process, which reduces the number of acidic groups on fiber surfaces. This low surface charge led to the agglomeration of LCNFs, resulting in a huge variability in fiber distribution and final film properties. While testing the OP of neat LCNF films, some of the samples randomly failed due to the extremely high oxygen transmission rates (typically >3000 g/m^2 day) and even those passed exhibited a coefficient of variation of 36% (Figure 1a). The agglomeration phenomenon of OCC-LCNFs and huge standard deviation in the final properties of films were also reported by other research groups. Copenhaver et al. (2021) reported the agglomerated morphology of OCC-LCNFs after spray drying.[24] Kelly et al. (2021) observed the huge randomness in peel strength values of OCC-derived LCNF applied as an adhesive between two paper substrates.[33] These reports and our observation led us to the conclusion that the suspension of LCNFs must be stabilized before film formation.

The adsorption of long polymeric chains on the surface of nanoparticles, which can act as a barrier between nanoparticles, is one of the common strategies for stabilizing nanoparticle suspensions.[34] If the polymer surface is charged, that is, a polyelectrolyte, the repulsion between the polymers can also ameliorate the stability of the whole suspension. This idea prompted us to incorporate CMC into our LCNF suspension as CMC can form hydrogen bonding with the cellulose, and the carboxylate group in CMC can provide negative charge. Being nearly charge-neutral, OCC-LCNFs had a greater potential of CMC adsorption than charged CNFs as there was no repulsive force between LCNFs and CMC chains caused by the same type of charge. CMC, on the other hand, can provide carboxylate groups that can serve as an active site for crosslinking that is detailed in the latter portion of this study. As we increased the proportion of CMC from 1 to 5 wt % relative to the mass of LCNFs, the zeta potential of the suspension showed a gradual decrease (Figure 1b) that can be related to the high stability of the overall suspension. Even 1% addition of CMC to LCNF suspension changed the zeta potential from −3.83 to −25.50 mV due to the high surface charge of CMC chains.

The addition of CMC to LCNF suspension changed the rheology of the suspension as well. The complex viscosity change over shear rate is an important parameter that can control the processing and final film properties. From Figure 1c, it was apparent that the complex viscosity of the LCNF suspension decreased with increasing shear rate, indicating the shear-thinning characteristic of the LCNF suspension. This behavior is a well-studied phenomenon for CNF-containing

https://doi.org/10.1021/acssuschemeng.2c06683
ACS Sustainable Chem. Eng. 2023, 11, 3720−3731

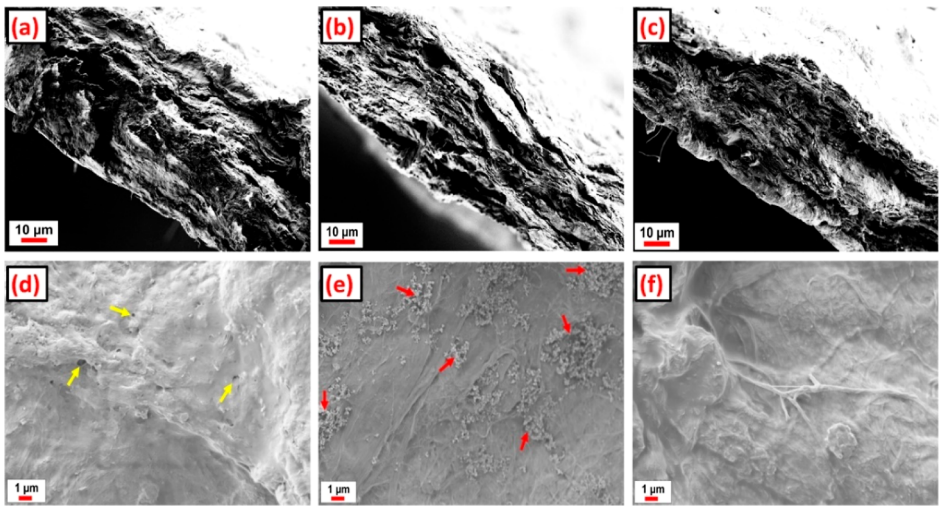

Figure 3. SEM images of cross-sections (a,b,c) and surfaces (d,e,f) of neat 3% CMC sLCNF films (a, d) and after treating at 0.3 wt % alum (b,e) and 0.3 wt % PAE solution baths.

suspensions.[35] When there is no shear stress, the LCNFs are entangled and attracted to each other through hydrogen bonding and van der Waals force, which eventually disentangle and become free to move at high shear rates.[36] As expected, with the addition of CMC, the viscosity gradually decreased due to the inhibition of particle aggregation, resulting in a gradual increase in filtration time with the gradual increase of the CMC percentage (Figure 1b). Therefore, the benefit of CMC addition was counteracted by the longer dewatering time compelling us to select an optimum amount of CMC addition. In this study, 3 wt % CMC was determined as the most optimum concentration as it maintained a sufficient zeta potential for a stable colloidal suspension (−30 mV) with a filtration time (∼15 min) close to that of a BSK-CNF suspension with similar parameters (∼12 min). In the following parts of this paper, we used this 3% CMC-stabilized LCNFs, which we referred to as "sLCNF".

Mechanism of Crosslinking and Microstructure Analysis of the Films. As mentioned in the preceding section, the addition of 3 wt % CMC to the OCC-LCNF suspension neither improved nor deteriorated the OP values of the films. However, the presence of carboxylate groups created the opportunity to crosslink the fibrils either by an ionic interaction or by covalent bonding to improve the gas barrier properties and mechanical strength of the films. For the ionic interaction, a trivalent ion Al^{3+} (from alum solution) was utilized to replace the Na^{+} group in CMC during the soaking process. The presence of a trivalent ion in the wet mat can bring the fibrils closer through an electrostatic interaction during the drying process, resulting in a more compact system.[37] In contrast, PAE is a well-established wet strength resin used in the paper industry. Obokata & Isogai (2007) first reported the mechanism by which PAE improved the wet strength of cellulose sheets.[38] In brief, the PAE chain is adsorbed onto the anionic carboxylate group of the cellulose fiber, and after the curing process at a high temperature, a new ester bond is formed between the cationic azetidinium group and the anionic carboxylate group of the cellulose fiber (Figure 2a). In addition to crosslinking with cellulose fibers, PAE chains can self-crosslink to some extent through a similar ester linkage as PAE chains contain carboxylic acid groups at the end of their chains. This crosslinking may even happen at room temperature, albeit at a slower rate.[15] Sharma & Deng (2016) also reported that this crosslinking not only improved the wet strength but also improved the dry strength of cellulose nanofibril films through a dual mechanism of crosslinking and hornification that occurred during the curing process at a high temperature.[39] A recent report also described a similar crosslinking mechanism between the CMC and PAE chains, which is more indicative of our system under study.[40]

To confirm if a similar ester linkage occurred in our films, we performed FTIR analysis as illustrated in Figure 2b,c. However, due to the presence of lignin and other additive materials in OCC-LCNFs, the FTIR spectra of pristine LCNF films showed a wide range of functional groups, including the majority of the functional groups expected to be present after crosslinking. As a result, we had to normalize all the spectra by the invariant cellulose peak at 1024 cm^{-1} to at least have a relative understanding of the existence of various functional groups. First, the characteristic broad bands of −OH stretching (∼3300 cm^{-1}), −CH stretching (∼2900 cm^{-1}), and −CO stretching (∼1050 cm^{-1}) for cellulose fibers were observed across the entire scanning wavelength (Figure 2b). In addition to cellulose peaks, two distinct peaks were also visible at 1510 and 1590 cm^{-1} linked with the C═C stretching of aromatic rings present in lignin.[24] As a result, the peak of the sodium carboxylate group (∼1590 cm^{-1}) after the addition of 3 wt % CMC to LCNF film overlapped with the pure LCNF film at that point. However, the slight increase in relative intensity is visible in Figure 2c. On the other hand, there was no difference between sLCNF and alum-treated films (the sLCNF treated in 0.3 wt % alum or 0.3 wt % PAE bath was taken as a representative for all alum-treated and PAE-treated films, respectively), even after normalizing the curves, as an ionic interaction was not anticipated to modify or form new chemical bonding. The most distinct curve was demonstrated by the PAE-treated film. A sharp peak (Figure 2c) with a greater relative intensity at 1740 cm^{-1} was a clear representation of ester linkage in the film. Intriguingly, a new peak at ∼1710 cm^{-1} appeared for PAE-treated films, which could be associated with the carboxylic acid group present at the end of some of the PAE chains.[38] The sharp peaks at 1645 and 1547 cm^{-1} represented the amide in PAE chains, further confirming the presence of PAE in the system.

https://doi.org/10.1021/acssuschemeng.2c06683
ACS Sustainable Chem. Eng. 2023, 11, 3720−3731

Table 1. Density, Thickness, EMC, WCA, and SFE Values of 3 wt % CMC-Stabilized LCNF (sLCNF) Films, as Well as Alum/PAE-Treated sLCNF Films

		0.1 wt % bath		0.3 wt % bath		0.5 wt % bath	
	sLCNF	alum	PAE	alum	PAE	alum	PAE
density (g/cc)	0.98 (1.4)[a]	0.96 (2.6)	1.10 (2.2)	0.96 (1.8)	1.15 (0.9)	0.98 (1.3)	1.12 (5.3)
thickness (μm)	70 (2.2)	68 (2.8)	57 (1.3)	68 (1.2)	51 (5.1)	65 (16.5)	58 (10)
EMC (%)	7.14 (0.3)	7.25 (3.3)	5.8 (0.5)	7.28 (0.1)	5.0 (6.9)	7.33 (0.5)	5.26 (4.3)
WCA (°)	82.7 (11.3)	91.1 (12.1)	92.7 (15.2)	90.4 (11.4)	96.2 (8.0)	90.3 (14.3)	92.2 (5.4)
SFE (mN/m)	33.3 (27.6)	32.3 (31.2)	30.6 (33.0)	33.6 (21.0)	29.1 (17.2)	28.8 (47.6)	30.7 (17.8)

[a]The values in parenthesis indicate the coefficient of variation.

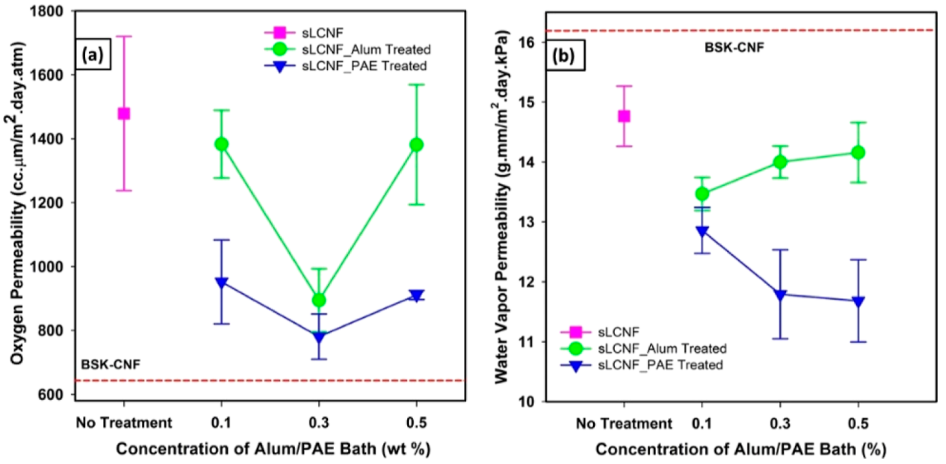

Figure 4. Changes in oxygen (a) (23 °C and 80% relative humidity) and water vapor (23 °C and 100/50% relative humidity difference) and (b) permeability values of 3 wt % CMC-containing LCNF films (sLCNF) before and after treating in different concentrations of alum and PAE bath.

Figure 3a–f illustrates the morphological changes on the surface and cross-section of the films induced by the ionic interaction and covalent bonding using a SEM. From the cross-sectional images (Figure 3a–c), the lamellar structure of OCC-derived LCNF films was evident, which is regarded as a characteristic structure in the cross-section of CNF films and has been reported by many other researchers.[41,42] Image analysis revealed an average sLCNF thickness of 61 ± 4 μm, while those of the films treated with alum or PAE were 44 ± 8 and 39 ± 5 μm, respectively. Although the thickness reduction of alum- and PAE-treated films could be caused by the enhanced interaction by crosslinking, the soaking of the wet mat in crosslinking baths followed by extended cold pressing could also contribute toward the vertical shrinkage. The thickness measurement with a micrometer on the wider area of the films also suggested a similar trend as listed in Table 1. However, the most prominent features were identified on the surface SEM images (Figure 3d–f). Nanoscale pores with an average diameter of 372 ± 220 nm were detected on the surface of untreated sLCNF films. At the same magnification, no such pores were visible for alum-treated and PAE-treated films, leading us to the expectation of lower oxygen gas permeability of those films. Moreover, only the alum-treated films showed a unique crystal structures on the surface. That crystal deposition is most likely caused by the physically entrapped Al^{3+} ions that turned into crystals after the evaporation of water.

Oxygen and Moisture Barrier Properties of the Crosslinked Films. The OP value of the 3 wt % CMC sLCNF film was found to be 1478 cc.μm/m^2.day.atm at 80% relative humidity, which was more than 2 times higher than that of the BSK-CNF films produced following the same procedure. One point worth mentioning here is that almost all lignocellulosic materials have an excellent oxygen barrier at low relative humidity,[43,44] for example, 50%, but exponentially lose this feature at a high relative humidity motivating us to select 80% relative humidity for oxygen transmission rate testing. The higher OP of sLCNF films in this study could be attributed to the presence of lignin or other foreign substances, including dyes, and adhesives, which can considerably disrupt the interfibrillar interaction or generate interfacial pores that facilitate the passage of oxygen. To strengthen the interaction between fibrils and reduce the micropores in films, we introduced Al^{3+} (from the alum solution) as an ionic interaction species with negatively charged carboxylate groups and PAE as a covalent crosslinking agent. As shown in Figure 4a, alum and PAE significantly reduced the OP values. However, PAE-treated films showed a considerably lower permeability than the alum-treated ones. On average, alum-treated films showed 18% less OP than the sLCNF films, whereas the PAE-treated ones showed a 40% reduction. The higher reduction by the PAE can be attributed to the higher density and less susceptibility to moisture in PAE-treated films as shown in Table 1. PAE-treated films, on average, showed 16% higher density than the alum-treated ones, leading to a less porous system that eventually blocks the oxygen molecules' movement through the films.[45] Moreover, PAE-treated films showed 27% lower EMC than the alum-treated samples, resulting in a more moisture sorption in the latter one. The higher moisture sorption can cause swelling of the fibrils disrupting the chain linkage and working as a medium for oxygen dissolution, facilitating the oxygen transfer.[46,47] Aside

https://doi.org/10.1021/acssuschemeng.2c06683
ACS Sustainable Chem. Eng. 2023, 11, 3720−3731

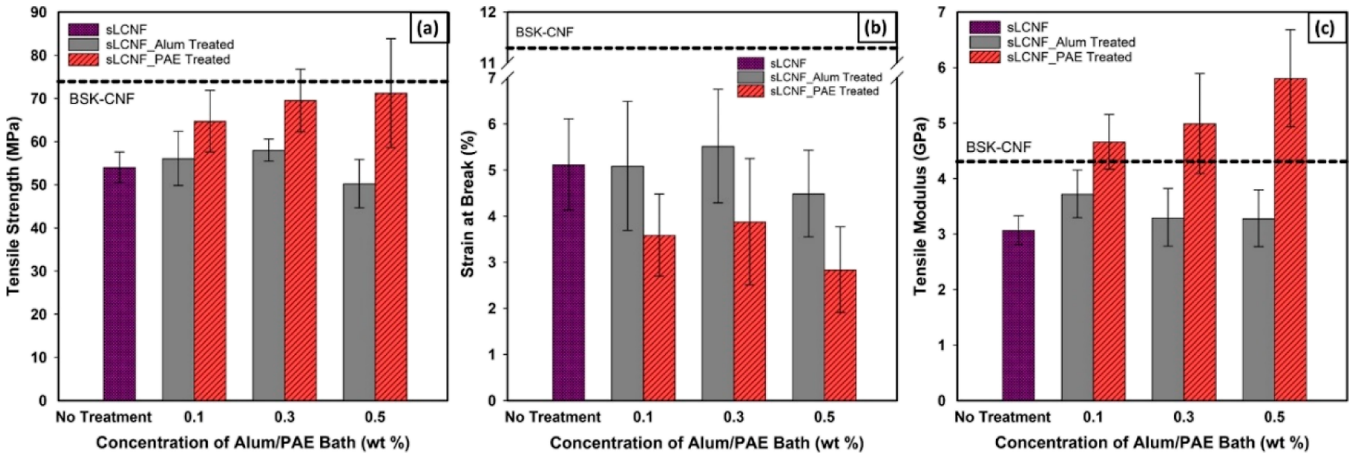

Figure 5. Tensile strength (a), strain at break (b), and modulus (c) of 3% CMC-loaded LCNF (sLCNF) films and corresponding mechanical properties after treating at different concentrations of an alum/PAE bath. The dashed lines indicate the corresponding values of bleached softwood Kraft pulp-produced CNF (BSK−CNF) films.

from the crosslinker type, the concentration of the alum/PAE bath significantly controlled the OP values. The concentration of the alum/PAE bath did not exhibit a linear relationship with the OP values. While treating at a 0.3 wt % bath showed the lowest OP values which were very comparable with the OP value of BSK-CNF films prepared similarly (630 cc·μm/m^2.day.atm), the OP values increased again soaking at 0.5 wt % bath for both crosslinkers turning 0.3 wt % as the most optimum one. The reason for this increase was not very clear and needs a detailed study. However, one potential explanation is that at 0.3 wt %, the crosslinkers might have a maximum crosslinking density and efficiency. Beyond that concentration, accumulation of non-interacted alum or unreacted PAE occurred, negatively affecting the overall oxygen barrier system. The OP of the films treated in a 0.3 wt % alum or a 0.3 wt % PAE bath was lower than most of the petroleum-based packaging materials, including polyethylene terephthalate, polyethylene, and polypropylene.[48]

In terms of water vapor barrier properties, LCNF films were more advantageous due to the presence of a greater amount of lignin than the BSK-CNF films. The vapor sorption of cellulose nanomaterial films is, in general, mostly controlled by the surface properties rather than the core.[48] Consequently, the presence of lignin in the surface layer works as a strong barrier to water molecules, thereby minimizing the overall absorption from the environment. Even sLCNF films without any crosslinking showed 10% lower WVP than the BSK-CNF films. Notably, alum treatment to the films did not appreciably alter the WVP values. Although treating at a 0.1 wt % alum bath slightly reduced the WVP (9%) compared with the sLCNF films, there was a gradual increase in WVP beyond that point. In a previous study from our group, it was shown that the addition of alum to the bulk CNF and LCNF suspension can significantly reduce the liquid water permeability of the films.[37] In this study, the liquid WCA values for alum-treated films were also higher compared to sLCNF films as listed in Table 1. However, they behaved differently for water vapor, and the reason for that might be associated with the interaction between water vapor and the surface alum crystals. On the other hand, PAE-treated films showed excellent water vapor barrier properties. On average, the PAE-treated films showed 18% lower WVP than the sLCNF films. The reason for this reduction can be attributed to the reduced porosity on the surface, the loading of the more hydrophobic portion from PAE to the film, and the ester linkage itself.[15] As cellulose-based materials are inherently hydrophilic, it is a major challenge for the commercialization of such materials to have low water vapor permeability. This study demonstrates that the addition of lignin and chemical crosslinking can reduce the water vapor permeability of films more effectively than BSK-CNF films, while maintaining a competitive oxygen barrier at high relative humidity. In Tables S1 and S2, the OP and water vapor permeability values of the films studied here are compared with the values of some other biobased and petroleum-based packaging materials, respectively.

Mechanical Properties. Along with high gas barrier properties, sufficient mechanical properties are desired for packaging films. Figure 5a−c depicts the tensile strength, strain at break, and tensile modulus of all the formulations, respectively. In general, the high mechanical performance of CNF films originated from the strong interfibrillar interaction caused by the capillary forces during drying from the hydrocolloid system. One interesting point to be mentioned here from a recent review that the strong interfibrillar interaction in CNF-based materials may not be controlled by the hydrogen bonding as it is short-ranged in nature, rather controlled by the long-range van der Waals force between the fibrils.[12] The tensile strength and modulus of lignin-containing CNF films varied considerably in the literature. Rojo et al. (2015) studied the effect of residual lignin on the mechanical properties of CNF films and concluded that the mechanical properties of CNF films are insensitive to the residual lignin content as the negative effect of hydrogen bonding interruption was mitigated by the softening and binding behavior of lignin during high-temperature hot-pressing.[44] On the other hand, Amini et al. (2020) reported lower strength and modulus of OCC-LCNF films compared to BSK-CNF films, which is more consistent with our system.[30] In our study, we found that our sLCNF films showed 27 and 28% lower strength and modulus, respectively, than the BSK-CNF films. This lower value of OCC-LCNF films, opposite to virgin unbleached softwood Kraft pulp LCNF films, can be caused by the different impurities present in the films, which permanently interrupted the interfibrillar interaction without imparting any binding property as the residual lignin does through softening at a high temperature. Moreover, although both BSK-CNFs

https://doi.org/10.1021/acssuschemeng.2c06683
ACS Sustainable Chem. Eng. 2023, 11, 3720−3731

and OCC-LCNFs are prepared at 90% fines content, the morphological properties of the two systems are essentially different, leading to differences in mechanical properties.

It is quite evident from Figure 5a–c and statistical analysis that the crosslinker type significantly influenced the mechanical properties. These differences existed even after density normalization of the strength and modulus. Therefore, the changes in properties were caused by crosslinking itself. In general, alum-treated samples did not show any significant differences in tensile properties compared to sLCNF films. Li et al. also reported that the tensile strength and modulus were insensitive to the ionic interaction with a copper ion (Cu^{2+}).[49] This can be attributed to the reversible and weak nature of the ionic interaction, especially in a system where only 3 wt % CMC was used as the anionic site to attract cationic Al^{3+}. Benefits in mechanical properties from the ionic interaction can be anticipated in a highly charged system like 2,2,6,6-tetramethylpiperidine-1-oxyl(TEMPO)-oxidized CNF as reported previously.[50]

PAE is one of the widely used polymers in paper industries to improve the wet strength of paper-based materials.[51] Therefore, PAE significantly improved the tensile strength and modulus of sLCNF films, even in a dry state. On average, PAE-treated films showed 28% higher tensile strength and 68% higher modulus than untreated films. Even treating at a 0.1 wt % PAE bath turned the sLCNF films stiffer than the BSK-CNF films prepared similarly. The main driving force for this improvement can be attributed to the new covalent bonds created by the reaction between azetidinium groups and carboxylate groups.[39] The other factor that can slightly contribute toward improved strength is the low EMC of PAE-treated films that protected the compact hydrogen bonding between fibers from moisture. Interestingly, the increase in tensile strength continued from the 0.3 wt % PAE bath treatment to the 0.5 wt % PAE bath treatment as opposed to barrier properties, although the density decreased in that range, indicating that the unreacted or self-crosslinked PAE chains did not affect the tensile properties rather it contributed toward the improvement of strength and modulus. Tayeb & Tajvidi (2018) also reported a similar observation as their PAE uncured CNF films showed higher strength than the neat CNF films.[15] However, the trade-off for covalent crosslinking was observed in tensile strains. Evidently, the linkage between fibers restricts the mobility of fibers, hence diminishing the flexibility of the films. PAE-treated films, on average, showed 33% lower strain than the sLCNF films, which in turn showed almost half of the strain of BSK-CNF films (11.2%). The wet strength measurement data of PAE- and alum-treated films (Figure S3) followed an exactly similar trend for strength, strain, and modulus with lower absolute values in strength and modulus and higher absolute values in strain due to the effect of plasticization induced by liquid water.[15]

UV–Vis Transmittance. The presence of phenolic structures in lignin is primarily responsible for the well-known UV protectiveness of LCNF films.[52] Generally, the UV region (200–400 nm) is divided into three major sub-regions: UV-A (320–400 nm), UV-B (280–320 nm), and UV-C (200–280 nm). In all previous studies, lignin-containing cellulose nanofibril films were reported to block different regions of UV lights depending on the percentage of lignin and lignin types.[52,53] In our study, the LCNF films showed almost zero percent transmittance (Figure 6) in the entire UV-A, UV-B, and UV-C regions, that is, complete UV-shielding performance of the films. This complete blockage of UV light can be attributed to the high percentage of residual lignin in our LCNF films (16.7%). Such high UV blocking is important for food packaging applications to stop the generation of oxygen free radicals and prevent the oxidation of lipids and degradation of antioxidants and vitamins.[54]

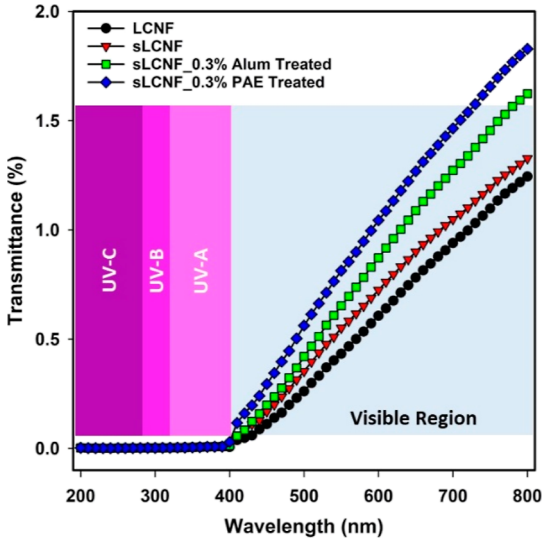

Figure 6. UV–vis spectra of neat LCNF, 3 wt.% CMC sLCNF before and after treating in a 0.3 wt % alum and PAE bath; all the curves overlapped in the UV region (200–400 nm) appearing as a single curve.

As a trade-off of high lignin content, the visible light transmittance of our films was very low. All films showed transmittance below 2%. This low transmittance of visible light can be attributed to the high content of residual lignin that not only absorbed light but also caused the scattering of light from the particle surfaces.[52] The presence of different foreign substances can also impact the absorbance of light. Within this 2% transmittance, however, there was a trend between different samples. The increased transmittance order between the samples were sLCNF_0.3% PAE treated > sLCNF_0.3% alum treated > sLCNF > LCNF. This trend is expected as it is well aligned with the thickness reduction of films, that is, the lower the thickness, the higher the transmittance.

CONCLUSIONS

Using an OCC as a starting fiber source results in a lower cost and energy demand to produce a robust gas barrier and a UV-protective film based on nanoscale lignocellulose. The OCC-LCNF suspension was colloidally unstable and caused variability in OP values. The addition of 3 wt % CMC based on cellulose to the LCNF suspension adequately stabilized the OP values. However, the OP value was considerably greater than that of the corresponding BSK-CNF films at 80% relative humidity. Treating films in a 0.3 wt % alum bath or a 0.3 wt % PAE bath reduced the OP values to 894 and 780 cc·μm/m^2.day.atm, respectively. In general, covalent crosslinking was more suitable for high gas barriers and mechanical strength. However, the drawback of covalent bonding was the reduction in strain at break. The thermal stability was decreased by the addition of CMC, which was later improved by the alum treatment. PAE-treated films were also more prone to the thermal degradation. All films studied here showed complete

https://doi.org/10.1021/acssuschemeng.2c06683
ACS Sustainable Chem. Eng. 2023, 11, 3720–3731

UV shielding due to high lignin content. This work has shown that OCC-derived LCNFs can give competitive properties for food packaging compared to its BSK pulp-derived counterpart. However, a lot of unknown foreign substances present in the OCC-LCNF can cause contamination to food items for food packaging applications. Therefore, future research direction should involve a thin coating or lamination of a very thin layer of pure CNF, LCNF, or any non-toxic biopolymer on top of the OCC-LCNF film to avoid potential contamination during food contact.

■ ASSOCIATED CONTENT

Supporting Information

The Supporting Information is available free of charge at https://pubs.acs.org/doi/10.1021/acssuschemeng.2c06683.

SEM images of OCC-LCNFs, images of OCC-LCNF suspension and films before and after CMC addition, tensile test data in wet condition, thermal properties of the films, and oxygen and water vapor permeability values of some other biopolymers and petroleum-derived polymers (PDF)

■ AUTHOR INFORMATION

Corresponding Author

Mehdi Tajvidi − *School of Forest Resources, University of Maine, Orono, Maine 04469, United States; Paper Surface Science Program, University of Maine, Orono, Maine 04469, United States; Advanced Structures and Composites Center, University of Maine, Orono, Maine 04469, United States;* orcid.org/0000-0002-3549-1220; Email: mehdi.tajvidi@maine.edu

Authors

Ikramul Hasan − *School of Forest Resources, University of Maine, Orono, Maine 04469, United States; Paper Surface Science Program, University of Maine, Orono, Maine 04469, United States;* orcid.org/0000-0003-0841-354X

Jinwu Wang − *School of Forest Resources, University of Maine, Orono, Maine 04469, United States; Forest Products Laboratory, U.S. Forest Service, Madison, Wisconsin 53726, United States; Advanced Structures and Composites Center, University of Maine, Orono, Maine 04469, United States;* orcid.org/0000-0002-8363-1689

Douglas Bousfield − *Paper Surface Science Program, University of Maine, Orono, Maine 04469, United States;* orcid.org/0000-0003-0753-1288

Complete contact information is available at: https://pubs.acs.org/10.1021/acssuschemeng.2c06683

Author Contributions

The manuscript was written through contributions of all authors. All authors have given approval to the final version of the manuscript.

Notes

The authors declare no competing financial interest.

■ ACKNOWLEDGMENTS

The authors would like to thank Dr. William Gramlich for his help with the FTIR data and Dr. Emma Perry for helping with the SEM. This work was partially supported through the agreement 19-JV-11111124-062 between the U.S. Forest Service and the University of Maine, UMaine Paper Surface Science Program (PSSP). This project was also supported by the USDA National Institute of Food and Agriculture, McIntire-Stennis, Project #042120.

■ ABBREVIATIONS

CNM, cellulose nanomaterial; CNF, cellulose nanofibril; LCNF, lignin-containing cellulose nanofibril; OCC, old corrugated cardboard; OCC-LCNF, old corrugated carboard-derived lignin-containing cellulose nanofibril; BSK, bleached softwood Kraft; BSK-CNF, bleached softwood Kraft pulp-derived cellulose nanofibril; CMC, carboxymethyl cellulose; PAE, polyamide epichlorohydrin; sLCNF, stabilized lignin-containing cellulose nanofibril; EMC, equilibrium moisture content; WVTR, water vapor transmission rate; WVP, water vapor permeability; OTR, oxygen transmission rate; OP, oxygen permeability; ATR, attenuated total reflectance; FTIR, Fourier transform infrared spectroscopy; SEM, scanning electron microscope; TGA, thermogravimetric analysis

■ REFERENCES

(1) Song, E.-H.; Kang, B.-H.; Kim, T.-Y.; Lee, H.-J.; Park, Y.-W.; Kim, Y.-C.; Ju, B.-K. Highly Oriented Gold/Nanoclay−Polymer Nanocomposites for Flexible Gas Barrier Films. *ACS Appl. Mater. Interfaces* **2015**, *7*, 4778−4783.

(2) Eckert, A.; Rudolph, T.; Guo, J.; Mang, T.; Walther, A. Exceptionally Ductile and Tough Biomimetic Artificial Nacre with Gas Barrier Function. *Adv. Mater.* **2018**, *30*, 1802477.

(3) Yang, Y.-H.; Haile, M.; Park, Y. T.; Malek, F. A.; Grunlan, J. C. Super Gas Barrier of All-Polymer Multilayer Thin Films. *Macromolecules* **2011**, *44*, 1450−1459.

(4) Struller, C. F.; Kelly, P. J.; Copeland, N. J. Aluminum Oxide Barrier Coatings on Polymer Films for Food Packaging Applications. *Surf. Coatings Technol.* **2014**, *241*, 130−137.

(5) Priolo, M. A.; Gamboa, D.; Holder, K. M.; Grunlan, J. C. Super Gas Barrier of Transparent Polymer−Clay Multilayer Ultrathin Films. *Nano Lett.* **2010**, *10*, 4970−4974.

(6) Yu, J.; Ruengkajorn, K.; Crivoi, D.-G.; Chen, C.; Buffet, J.-C.; O'Hare, D. High Gas Barrier Coating Using Non-Toxic Nanosheet Dispersions for Flexible Food Packaging Film. *Nat. Commun.* **2019**, *10*, 2398.

(7) Kim, H.; Miura, Y.; Macosko, C. W. Graphene/Polyurethane Nanocomposites for Improved Gas Barrier and Electrical Conductivity. *Chem. Mater.* **2010**, *22*, 3441−3450.

(8) Priolo, M. A.; Holder, K. M.; Gamboa, D.; Grunlan, J. C. Influence of Clay Concentration on the Gas Barrier of Clay−Polymer Nanobrick Wall Thin Film Assemblies. *Langmuir* **2011**, *27*, 12106−12114.

(9) Walker, F.; Frelka, S.; Shen, B.; Chew, G.; Banick, K. M.; Grey, S.; Kim, M. S.; Dumesic, J. A.; Van Lehn, R. C.; Huber, G. W. Recycling of Multilayer Plastic Packaging Materials by Solvent-Targeted Recovery and Precipitation. *Sci. Adv.* **2020**, *6*, No. eaba7599.

(10) Lu, C.; Mai, Y.-W. Influence of Aspect Ratio on Barrier Properties of Polymer-Clay Nanocomposites. *Phys. Rev. Lett.* **2005**, *95*, 88303.

(11) Priolo, M. A.; Gamboa, D.; Grunlan, J. C. Transparent Clay−Polymer Nano Brick Wall Assemblies with Tailorable Oxygen Barrier. *ACS Appl. Mater. Interfaces* **2010**, *2*, 312−320.

(12) Wohlert, M.; Benselfelt, T.; Wågberg, L.; Furó, I.; Berglund, L. A.; Wohlert, J. Cellulose and the Role of Hydrogen Bonds: Not in Charge of Everything. *Cellulose* **2022**, *29*, 1−23.

(13) Moon, R. J.; Martini, A.; Nairn, J.; Simonsen, J.; Youngblood, J. Cellulose Nanomaterials Review: Structure, Properties and Nanocomposites. *Chem. Soc. Rev.* **2011**, *40*, 3941−3994.

(14) Fukuzumi, H.; Saito, T.; Iwata, T.; Kumamoto, Y.; Isogai, A. Transparent and High Gas Barrier Films of Cellulose Nanofibers Prepared by TEMPO-Mediated Oxidation. *Biomacromolecules* **2009**, *10*, 162−165.

(15) Tayeb, H.; Tajvidi, M. Barrier System via Self-Assembly of Colloidal Montmorillonite and Cross-Linking Resins on Nanocellulose Interfaces. *ACS Appl. Mater. Interfaces* **2019**, *11*, 1604−1615.
(16) Qin, S.; Pour, M. G.; Lazar, S.; Köklükaya, O.; Gerringer, J.; Song, Y.; Wågberg, L.; Grunlan, J. C. Super Gas Barrier and Fire Resistance of Nanoplatelet/Nanofibril Multilayer Thin Films. *Adv. Mater. Interfaces* **2019**, *6*, 1801424.
(17) Aulin, C.; Karabulut, E.; Tran, A.; Wågberg, L.; Lindström, T. Transparent Nanocellulosic Multilayer Thin Films on Polylactic Acid with Tunable Gas Barrier Properties. *ACS Appl. Mater. Interfaces* **2013**, *5*, 7352−7359.
(18) Dai, L.; Long, Z.; Chen, J.; An, X.; Cheng, D.; Khan, A.; Ni, Y. Robust Guar Gum/Cellulose Nanofibrils Multilayer Films with Good Barrier Properties. *ACS Appl. Mater. Interfaces* **2017**, *9*, 5477−5485.
(19) Song, Y.; Jiang, W.; Zhang, Y.; Ben, H.; Han, G.; Ragauskas, A. J. Isolation and Characterization of Cellulosic Fibers from Kenaf Bast Using Steam Explosion and Fenton Oxidation Treatment. *Cellulose* **2018**, *25*, 4979−4992.
(20) Hassan, M. L.; Bras, J.; Hassan, E. A.; Silard, C.; Mauret, E. Enzyme-Assisted Isolation of Microfibrillated Cellulose from Date Palm Fruit Stalks. *Ind. Crops Prod.* **2014**, *55*, 102−108.
(21) Alemdar, A.; Sain, M. Isolation and Characterization of Nanofibers from Agricultural Residues − Wheat Straw and Soy Hulls. *Bioresour. Technol.* **2008**, *99*, 1664−1671.
(22) Xiao, S.; Gao, R.; Gao, L.; Li, J. Poly(Vinyl Alcohol) Films Reinforced with Nanofibrillated Cellulose (NFC) Isolated from Corn Husk by High Intensity Ultrasonication. *Carbohydr. Polym.* **2016**, *136*, 1027−1034.
(23) Zambrano, F.; Marquez, R.; Jameel, H.; Venditti, R.; Gonzalez, R. Upcycling Strategies for Old Corrugated Containerboard to Attain High-Performance Tissue Paper: A Viable Answer to the Packaging Waste Generation Dilemma. *Resour. Conserv. Recycl.* **2021**, *175*, 105854.
(24) Copenhaver, K.; Li, K.; Lamm, M. E.; Walker, C.; Johnson, D.; Han, Y.; Wang, L.; Zhao, X.; Pu, Y.; Hinton, H.; Tekinalp, H.; Bhagia, S.; Ragauskas, A. J.; Gardner, D. J.; Ozcan, S. Recycled Cardboard Containers as a Low Energy Source for Cellulose Nanofibrils and Their Use in Poly(l -Lactide) Nanocomposites. *ACS Sustain. Chem. Eng.* **2021**, *9*, 13460−13470.
(25) Ashori, A.; Marashi, M.; Ghasemian, A.; Afra, E. Utilization of Sugarcane Molasses as a Dry-Strength Additive for Old Corrugated Container Recycled Paper. *Compos. Part B Eng.* **2013**, *45*, 1595−1600.
(26) Balea, A.; Sanchez-Salvador, J. L.; Monte, M. C.; Merayo, N.; Negro, C.; Blanco, A. In Situ Production and Application of Cellulose Nanofibers to Improve Recycled Paper Production. *Molecules* **2019**, *24*, 1800.
(27) Lal, S. S.; Mhaske, S. T. Old Corrugated Box (OCB)-Based Cellulose Nanofiber-Reinforced and Citric Acid-Cross-Linked TSP−Guar Gum Composite Film. *Polym. Bull.* **2021**, *78*, 885−915.
(28) Yousefhashemi, S. M.; Khosravani, A.; Yousefi, H. Isolation of Lignocellulose Nanofiber from Recycled Old Corrugated Container and Its Interaction with Cationic Starch−Nanosilica Combination to Make Paperboard. *Cellulose* **2019**, *26*, 7207−7221.
(29) Bilodeau, M.; Spender, J.; Van Heiningen, A. Methods for the Production of High Solids Nanocellulose; WO 2016172616 A1, 2016.
(30) Amini, E.; Hafez, I.; Tajvidi, M.; Bousfield, D. W. Cellulose and Lignocellulose Nanofibril Suspensions and Films: A Comparison. *Carbohydr. Polym.* **2020**, *250*, 117011.
(31) Hasan, I.; Wang, J.; Tajvidi, M. Tuning Physical, Mechanical and Barrier Properties of Cellulose Nanofibril Films through Film Drying Techniques Coupled with Thermal Compression. *Cellulose* **2021**, *28*, 11345−11366.
(32) Bian, H.; Chen, L.; Dai, H.; Zhu, J. Y. Integrated Production of Lignin Containing Cellulose Nanocrystals (LCNC) and Nanofibrils (LCNF) Using an Easily Recyclable Di-Carboxylic Acid. *Carbohydr. Polym.* **2017**, *167*, 167−176.
(33) Kelly, P. V.; Gardner, D. J.; Gramlich, W. M. Optimizing Lignocellulosic Nanofibril Dimensions and Morphology by Mechanical Refining for Enhanced Adhesion. *Carbohydr. Polym.* **2021**, *273*, 118566.
(34) González García, Á.; Nagelkerke, M. M. B.; Tuinier, R.; Vis, M. Polymer-Mediated Colloidal Stability: On the Transition between Adsorption and Depletion. *Adv. Colloid Interface Sci.* **2020**, *275*, 102077−12.
(35) Saarikoski, E.; Saarinen, T.; Salmela, J.; Seppälä, J. Flocculated Flow of Microfibrillated Cellulose Water Suspensions: An Imaging Approach for Characterisation of Rheological Behaviour. *Cellulose* **2012**, *19*, 647−659.
(36) Nechyporchuk, O.; Belgacem, M. N.; Pignon, F. Current Progress in Rheology of Cellulose Nanofibril Suspensions. *Biomacromolecules* **2016**, *17*, 2311−2320.
(37) Hossain, R.; Tajvidi, M.; Bousfield, D.; Gardner, D. J. Recyclable Grease-Proof Cellulose Nanocomposites with Enhanced Water Resistance for Food Serving Applications. *Cellulose* **2022**, *29*, 5623−5643.
(38) Obokata, T.; Isogai, A. The Mechanism of Wet-Strength Development of Cellulose Sheets Prepared with Polyamideamine-Epichlorohydrin (PAE) Resin. *Colloids Surfaces A Physicochem. Eng. Asp.* **2007**, *302*, 525−531.
(39) Sharma, S.; Deng, Y. Dual Mechanism of Dry Strength Improvement of Cellulose Nanofibril Films by Polyamide-Epichlorohydrin Resin Cross-Linking. *Ind. Eng. Chem. Res.* **2016**, *55*, 11467−11474.
(40) Azrak, S. M. E. A.; Gohl, J. A.; Moon, R. J.; Schueneman, G. T.; Davis, C. S.; Youngblood, J. P. Controlled Dispersion and Setting of Cellulose Nanofibril - Carboxymethyl Cellulose Pastes. *Cellulose* **2021**, *28*, 9149−9168.
(41) Österberg, M.; Vartiainen, J.; Lucenius, J.; Hippi, U.; Seppälä, J.; Serimaa, R.; Laine, J. A Fast Method to Produce Strong NFC Films as a Platform for Barrier and Functional Materials. *ACS Appl. Mater. Interfaces* **2013**, *5*, 4640−4647.
(42) Fein, K.; Bousfield, D. W.; Gramlich, W. M. Processing Effects on Structure, Strength, and Barrier Properties of Refiner-Produced Cellulose Nanofibril Layers. *ACS Appl. Polym. Mater.* **2021**, *3*, 3666−3678.
(43) Aulin, C.; Gällstedt, M.; Lindström, T. Oxygen and Oil Barrier Properties of Microfibrillated Cellulose Films and Coatings. *Cellulose* **2010**, *17*, 559−574.
(44) Rojo, E.; Peresin, M. S.; Sampson, W. W.; Hoeger, I. C.; Vartiainen, J.; Laine, J.; Rojas, O. J. Comprehensive Elucidation of the Effect of Residual Lignin on the Physical, Barrier, Mechanical and Surface Properties of Nanocellulose Films. *Green Chem.* **2015**, *17*, 1853−1866.
(45) Hossen, M. R.; Talbot, M. W.; Kennard, R.; Bousfield, D. W.; Mason, M. D.; Kennard, R. A Comparative Study of Methods for Porosity Determination of Cellulose Based Porous Materials. *Cellulose* **2020**, *27*, 6849−6860.
(46) Tayeb, H. A.; Bousfield, M.; Bousfield, D. Enhancing the Oxygen Barrier Properties of Nanocellulose at High Humidity: Numerical and Experimental Assessment. *Sustain. Chem.* **2020**, *1*, 198−208.
(47) Lagaron, J. M.; Catalá, R.; Gavara, R. Structural Characteristics Defining High Barrier Properties in Polymeric Materials. *Mater. Sci. Technol.* **2004**, *20*, 1−7.
(48) Wang, J.; Gardner, D. J.; Stark, N. M.; Bousfield, D. W.; Tajvidi, M.; Cai, Z. Moisture and Oxygen Barrier Properties of Cellulose Nanomaterial-Based Films. *ACS Sustain. Chem. Eng.* **2018**, *6*, 49−70.
(49) Li, K.; Skolrood, L. N.; Aytug, T.; Tekinalp, H.; Ozcan, S. Strong and Tough Cellulose Nanofibrils Composite Films: Mechanism of Synergetic Effect of Hydrogen Bonds and Ionic Interactions. *ACS Sustain. Chem. Eng.* **2019**, *7*, 14341−14346.
(50) Shimizu, M.; Saito, T.; Isogai, A. Water-Resistant and High Oxygen-Barrier Nanocellulose Films with Interfibrillar Cross-Linkages Formed through Multivalent Metal Ions. *J. Memb. Sci.* **2016**, *500*, 1−7.

https://doi.org/10.1021/acssuschemeng.2c06683
ACS Sustainable Chem. Eng. 2023, 11, 3720−3731

(51) Su, J.; Mosse, W. K. J.; Sharman, S.; Batchelor, W.; Garnier, G. Paper Strength Development and Recyclability with Polyamideamine-Epichlorohydrin (PAE). *BioResources* **2012**, *7*, 913−924.
(52) Farooq, M.; Zou, T.; Riviere, G.; Sipponen, M. H.; Österberg, M. Strong, Ductile, and Waterproof Cellulose Nanofibril Composite Films with Colloidal Lignin Particles. *Biomacromolecules* **2019**, *20*, 693−704.
(53) Li, P.; Sirviö, J. A.; Hong, S.; Ämmälä, A.; Liimatainen, H. Preparation of Flame-Retardant Lignin-Containing Wood Nanofibers Using a High-Consistency Mechano-Chemical Pretreatment. *Chem. Eng. J.* **2019**, *375*, 122050.
(54) Sirviö, J. A.; Ismail, M. Y.; Zhang, K.; Tejesvi, M. V.; Ämmälä, A. Transparent Lignin-Containing Wood Nanofiber Films with UV-Blocking, Oxygen Barrier, and Anti-Microbial Properties. *J. Mater. Chem. A* **2020**, *8*, 7935−7946.

https://doi.org/10.1021/acssuschemeng.2c06683
ACS Sustainable Chem. Eng. 2023, 11, 3720−3731